

Review

A Critical Review of Spinel Structured Iron Cobalt Oxides Based Materials for Electrochemical Energy Storage and Conversion

Hongyan Gao ¹, Shuai Liu ², Yafei Li ², Eric Conte ¹ and Yan Cao ^{1,2,*}

¹ Department of Chemistry, Western Kentucky University, Bowling Green, KY 42101, USA; hongyan.gao408@topper.wku.edu (H.G.); eric.conte@wku.edu (E.C.)

² College of Chemistry & Chemical Engineering, Anhui University, Hefei 230601, China; mayday_55555@163.com (S.L.); icyue@icloud.com (Y.L.)

* Correspondence: yan.cao@wku.edu; Tel.: +1-270-779-0202

Received: 1 October 2017; Accepted: 30 October 2017; Published: 6 November 2017

Abstract: Iron cobalt oxides, such as typical FeCo_2O_4 and CoFe_2O_4 , are two spinel structured transitional metal oxide materials with excellent electrochemical performance. As the electrodes, they have been widely applied in the current energy storage and conversion processes such as supercapacitors, Lithium-ion batteries and fuel cells. Based on synthesis approaches and controlled conditions, these two materials exhibited broad morphologies and nanostructures and thus distinct electrochemical performance. Some of them have shown promising applications as electrodes in energy storage and conversion. The incorporation with other materials to form composites further improved their performance. This review briefly summarized the recent applications of FeCo_2O_4 and CoFe_2O_4 in energy storage and conversion, current understandings on mechanisms and especially the relevance of morphologies and structures and composites to electrochemical performance. Some recommendations were finally put forward addressing current issues and future prospects on electrodes of FeCo_2O_4 and CoFe_2O_4 based materials in energy storage and conversion, implying there was still space to further optimize their performance.

Keywords: spinel iron cobalt oxides; composites; nanostructure and nanoengineering; electrochemistry; energy storage and conversion

1. Introduction

The severe environmental issues relative to the use of fossil fuels calls for the urgently demanding development of highly-efficient energy conversion and storage devices, such as fuel cells, supercapacitors and Lithium-ion batteries (LIBs) [1–3]. Despite the energy storage and conversion mechanisms may be different among these three devices, they still share fundamentally electrochemical similarities. All energy storage and conversion processes occur at the interface of electrode and electrolyte and the electron and ion transport are separated [4]. A simplified Ragone plot (Figure 1) can demonstrate domains of these energy storage and conversion systems differentially from traditional power systems such as combustion engine, turbines and regular capacitors. Among of them, fuel cells belong to high-energy systems as the anode and cathode are used to transfer charge and fuels undergo the redox reactions without involving the process of combustion, whereas supercapacitors belong to high-power system since supercapacitors stores electrical charges both at the electrode surface and in the bulk near the surface of the solid electrode. Lithium-ion batteries have intermediate power and energy characteristics. Electrode materials are the most important components for energy storage and conversion systems, which usually include three groups of popular electrode materials such as carbon materials, conducting polymers and transition metal oxides. It is remarkable that transition

metal oxides can be applied as electrode materials for these three major energy storage and conversion systems because of their relevance to redox reactions to some extent.

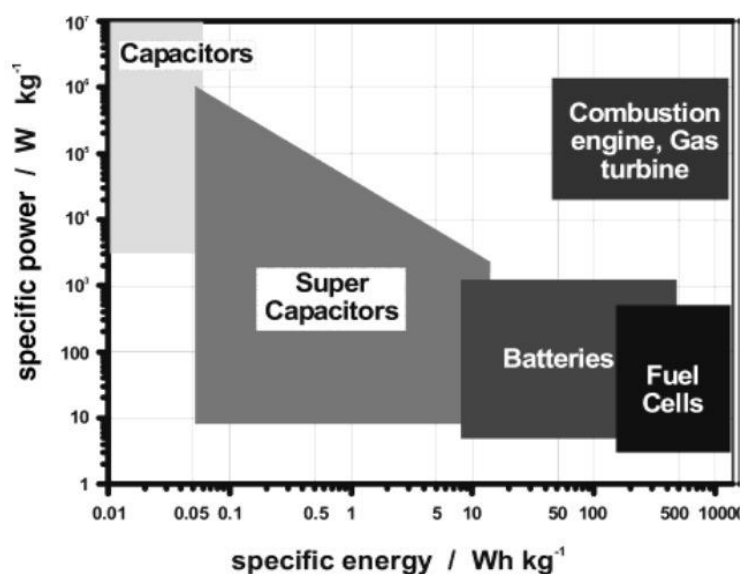


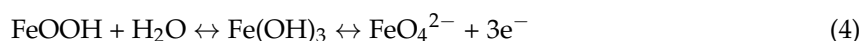
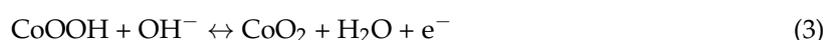
Figure 1. Simplified Ragone plot of the energy storage domains for the various electrochemical energy storage and conversion systems compared to an internal combustion engine and turbines and conventional capacitors [5].

Transition metal oxides possess several oxidation states that are favorable for rapid redox reactions, leading to efficient and high-quality energy storage and conversion systems. However, the single metal oxides such as NiO [5,6], Co_3O_4 [7–9] and MnO_2 [10] generally suffer from low conductive properties and unfavorable stability, which constrain the performance of energy storage and conversion systems. Nanostructures and composite engineering of materials are promising approaches to address issues of single metal oxides [11]. This is why the recent rise of binary metal oxides which were paid much attention in energy storage and conversion applications by virtue of their better conductivity and electrochemical performance. Among all these binary metal oxides, spinel cobaltites— $\text{M}_x\text{Co}_{3-x}\text{O}_4$ (M = Ni, Mn, Zn, Cu and so on)—have exhibited better characteristics in fuel cells, Li-ion batteries and supercapacitors [12–14]. Not only can the conductivity and electrochemical activity be improved but the toxicity and cost can be reduced through partly substituting the Co-content with other less-toxic and highly-performed metals. Iron can be a promising substitutable metal due to its abundance, non-toxic and excellent substitution performance. For example, FeCo_2O_4 and CoFe_2O_4 have been two widely investigated promising binary metal oxides as electrode materials for supercapacitors, fuel cells and Li-ion batteries.

Since FeCo_2O_4 and CoFe_2O_4 based electrodes store charges and convert energy mainly on their surface and near-surface bulky structures, high specific surface areas are specially required. Nanostructured materials can achieve much high specific surfaces, providing the shorter transport and diffusion path lengths for ions and electrons as well as more electroactive sites for energy storage and conversion. On the other hand, the fabrication of iron cobalt oxides based composite materials also is another strategy to enhance the performance of supercapacitors, Li-ion batteries and fuel cells, in conductivity, mechanical strength and specific surface areas. These have been presented in a large quantity of the recent literatures but to date, no reviews has summarized these two binary metal oxides. In this paper, nanostructures and morphologies of FeCo_2O_4 and CoFe_2O_4 and their relative composites materials as well as their corresponding performance were summarized and mechanisms of FeCo_2O_4 and CoFe_2O_4 on energy storage and conversion was proposed, the applications of FeCo_2O_4 and CoFe_2O_4 based materials as energy storage and conversion electrodes were discussed.

2. Application for Supercapacitors

According to the energy storage mechanism, supercapacitors can be further divided into two categories: the first is electrochemical double-layer capacitor (EDLC) which stores energy by accumulating charge in the electrode/electrolyte interface and the second is the pseudo-capacitors based on the fast and reversible redox reactions at electrochemically active sites [15,16]. Spinel cobaltites and ferrites materials, such as FeCo_2O_4 and CoFe_2O_4 , based materials can be used as the electrodes for pseudo-capacitors. They store charges both on the surface and in the bulk near the surface of the solid electrode where the Faradic reactions occur [17]. The energy storage mechanisms for pseudo-capacitors of FeCo_2O_4 and CoFe_2O_4 in alkaline solution can be described by the following equations [18]:



Several morphologies of FeCo_2O_4 and CoFe_2O_4 have been reported, addressing nanoparticles, nanowires, nanosheets and nanoshelled-microspheres. Direct growth of nanostructured FeCo_2O_4 and CoFe_2O_4 electrode materials have been reported recently on highly conductive substrates such as the nickel foam and the stainless steel, avoiding the use of binder and additives to exposure almost all available surface involved in energy storage and conversion process. In addition, several other materials which also own the electrochemical capacitance properties such as carbon materials, metal oxides and conducting polymers have been combined with iron cobalt oxides to fabricate composite material electrodes. As expected, these composited materials displayed an enhanced performance and showed synergistic effects in supercapacitor applications. The currently available morphologies and composites of FeCo_2O_4 and CoFe_2O_4 were briefly summarized in Table 1.

Table 1. Summary of iron cobalt oxides based materials for supercapacitor applications.

Materials	Synthetic Method	Potential Window	Specific Capacitance	Cycling Stability	Ref.
FeCo_2O_4 nanowires/NF	Hydrothermal	0 to 0.55 V (vs. Hg/HgO)	428 F g^{-1} (5 mV s^{-1})	142% retention after 2000 cycles	[18]
CoFe_2O_4 nanoparticles	Hard-templating	-1.0 to 0.5 V (vs. Hg/HgO)	142 F g^{-1} (2 mV s^{-1})	71.8% retention after 1000 cycles	[19]
CoFe_2O_4 hollow microspheres	Hydrothermal	0 to 0.4 V (vs. Ag/AgCl)	1790 F g^{-1} (2 A g^{-1})	98% retention after 500 cycles	[20]
CoFe_2O_4 nanoflakes/SS	Chemical bath deposition	-1.0 to -0.2 V (vs. SCE)	366 F g^{-1} (5 mV s^{-1})	90.6% retention after 1000 cycles	[21]
FeCo_2O_4 nanoflakes/NF	Hydrothermal	0 to 2.5 V (two-electrode systems)	433 F g^{-1} (0.1 A g^{-1})	62.5% retention after 2500 cycles	[22]
CoFe_2O_4 nanosheets/NF	Hydrothermal	0-0.4 V (vs. Ag/AgCl)	503 F g^{-1} (2 A g^{-1})	98% retention after 5000 cycles	[23]
CoFe_2O_4 nanomesh/NF	Hydrothermal	0 to 0.6 V (vs. SCE)	1426 F g^{-1} (1 A g^{-1})	92.6% retention after 3000 cycles	[24]
FeCo_2O_4 submicron-tube/NF	Chemical bath deposition	-0.2 to 0.6 V (vs. Ag/AgCl)	1254 F g^{-1} (2 mA cm^{-2})	91% retention after 5000 cycles	[25]
CoFe_2O_4 nanoparticles	Solution combustion	-1.1 to 0 V (vs. Hg/HgO)	195 F g^{-1} (1 mV s^{-1})	67% retention after 3000 cycles	[26]
CoFe_2O_4 /graphene/PANI	Hydrothermal + polymerization	-0.8 to 0.2 V (vs. Hg/HgO)	1133.3 F g^{-1} (1 mV s^{-1})	96% retention after 5000 cycles	[27]

Table 1. Cont.

Materials	Synthetic Method	Potential Window	Specific Capacitance	Cycling Stability	Ref.
FeCo ₂ O ₄ -Tube/MnO ₂ nanosheets	Chemical bath deposition + Hydrothermal	0 to 0.6 V (vs. Ag/AgCl)	3.3 F cm ⁻² (1 mA cm ⁻²)	94% retention after 2000 cycles	[28]
CoFe ₂ O ₄ /MnO ₂ nanosheet arrays	Hydrothermal	-0.2 to 0.4 V (vs. Ag/AgCl)	3.59 F cm ⁻² (2 mA cm ⁻²)	91.5% retention after 2250 cycles	[29]
FeCo ₂ O ₄ /MnO ₂ nanosheet arrays	Hydrothermal	0 to 0.45 V (vs. SCE)	2491.8 F g ⁻¹ (4 mA cm ⁻²)	87.2 retention after 5000 cycles	[30]
CoFe ₂ O ₄ /FeOOH	Hydrothermal	-0.2 to 0.3 V (vs. Hg/HgO)	332.4 F g ⁻¹ (0.5 A g ⁻¹)	91.3% retention after 1000 cycles	[31]
CoFe ₂ O ₄ /RGO/PANI	Solution combustion + polymerization	-0.174 to 0.926 V (vs. SHE)	239 F g ⁻¹ (1.5 A g ⁻¹)	100% retention after 1000 cycles	[32]

SS: stainless steel; NF: nickel foam; RGO: reduced graphene oxide; PANI: polyaniline.

According to the data listed in Table 1, showed 3D-structured iron cobalt oxides seemed to have higher specific capacitance than 1D and 2D structures. Remarkably, Wang et al. [20], successfully fabricated multi-shelled CoFe₂O₄ hollow microspheres with a controllable number of layers from 1 to 4 via a simple facile one-step hydrothermal method using cyclodextrin as a template. The representative figures multi-shelled CoFe₂O₄ hollow microspheres are shown in Figure 2. The specific capacitance of triple-shelled CoFe₂O₄ hollow microspheres reached 1790 F g⁻¹ at a current density of 2 A g⁻¹, which was the highest capacitance among CoFe₂O₄ electrodes. FeCo₂O₄ submicron-tube arrays grown on nickel foam served as binder/additive-free electrodes for supercapacitor [25]. The optimized specific capacitance of FeCo₂O₄-tube electrode reached 1254 F g⁻¹ at 2 mA cm⁻². Both of these two 3D-structured materials can maintain high capacitances at 98% of their original specific capacitances after 500 cycles and at 91% after 5000 cycles, respectively. Unlike other binary metal oxides such as NiCo₂O₄ [33,34], CuCo₂O₄ [35] and ZnCo₂O₄ [36], the 3D micro-structured and submicron-structured iron cobalt oxides even exhibited relatively high specific capacitances and cycling-stability compared to their 1D and 2D nano-structured counterparts such as nanowires or nanosheets. The excellent performance may contribute to unique morphology and high porosity of these materials which can provide a large electrode/electrolyte interface. The 3D-structured frames likely constructed a cross-linking electron transport path and also an ion reservoir for electrolyte ion accumulation. Furthermore, 3D-structured frames had better structural mechanical stability, realizing a better cycling-stability. Pendasheh et al. [18], fabricated FeCo₂O₄ porous wires with an average edge length about 200 nm which was in submicron scale supported on the nickel foam and achieved 407 F g⁻¹ at 10 mV s⁻¹. Interestingly, cycling for 2000 cycles seemed to electro-activate the material and to achieve the pore opening (Figure 3), leading a subsequent increase in the capacitance up to 610 F g⁻¹, which was a significant characteristic of the electrode materials for supercapacitor. In addition, we noticed that most of iron cobalt oxides based materials grown on highly conductive substrates, such as the nickel foam, exhibited the better cycling stability (more than 90% retention after 2000 cycles) than those on powder materials. This should be attributed to that the electrical connection of the electrode materials to the Ni foam without any binder or conductive agents can enhance the long-term performance of the hybrid electrodes. Moreover, the enhanced electrical conductivity of bimetallic iron cobalt oxides has been confirmed by previous works and ours. Our group directly fabricated ultrathin CoFe₂O₄ nanosheets on the excellent-conductive nickel foam free of binders and exhibited better electrical conductivity than those of both its corresponding monometallic oxides. This approach clearly facilitated both the better charge transfer and ions diffusion [23]. The as-prepared FeCo₂O₄ nanowires also exhibited similar results [18] (Figure 4).

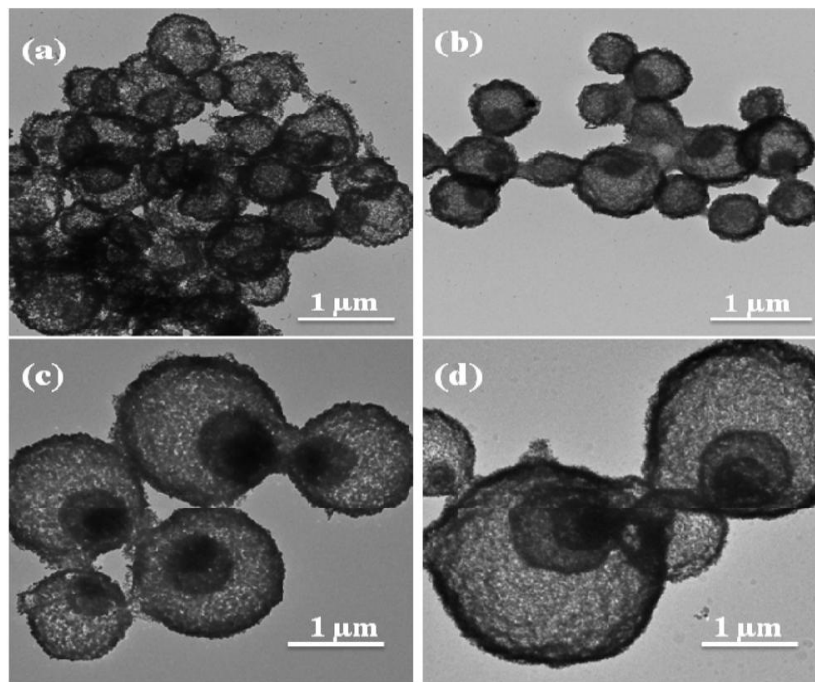


Figure 2. Transmission electron microscope (TEM) images of CoFe_2O_4 multi-shelled hollow microspheres after calcination at $550\text{ }^\circ\text{C}$: (a) single-shelled, (b) double-shelled, (c) triple-shelled, (d) quadruple-shelled hollow spheres [20].

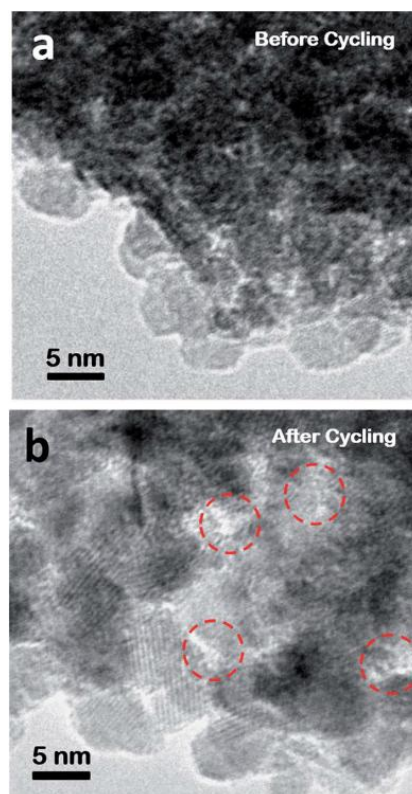


Figure 3. TEM images of the nanostructured FeCo_2O_4 micro-wires before (a) and after 2000 cycles (b). The red circles show regions in which the pores are enlarged, and the lattice fringes become diminished [18].

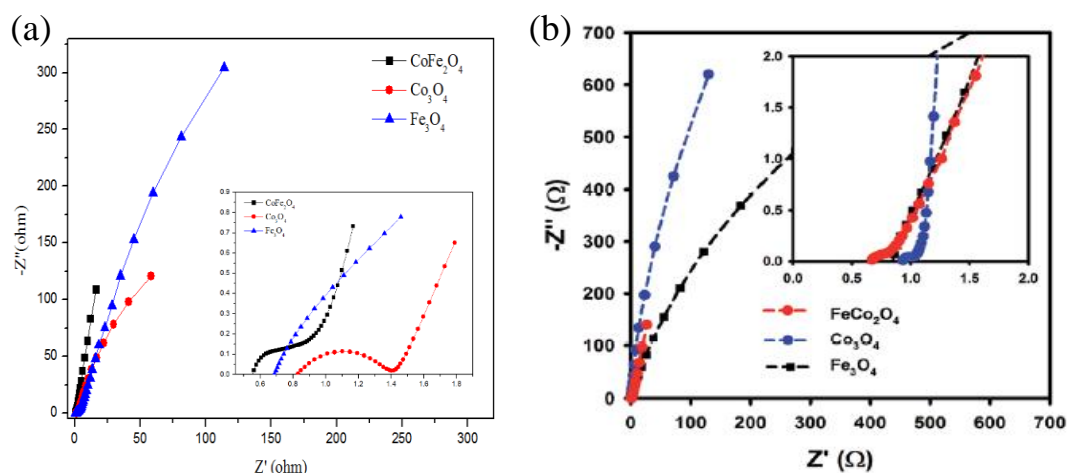


Figure 4. Nyquist plots of (a) the CoFe_2O_4 nanosheets [23] and (b) FeCo_2O_4 nanowires [18] with their corresponding monometallic oxides.

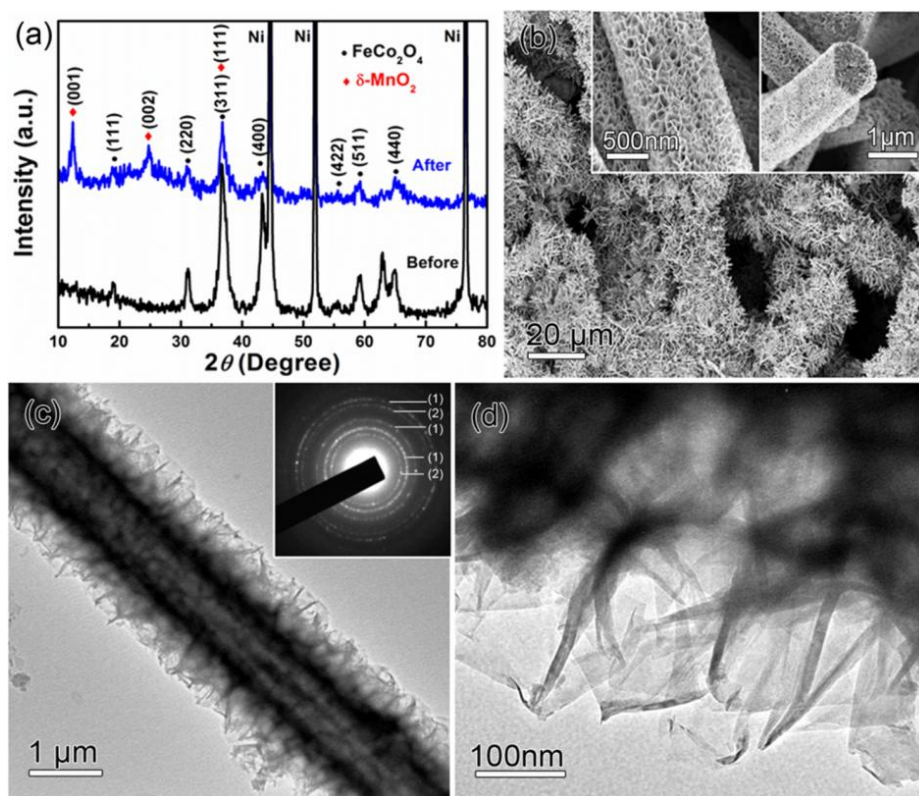


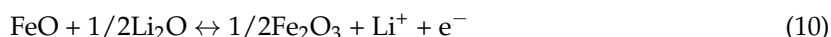
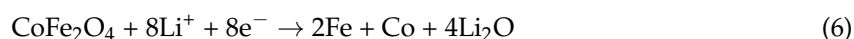
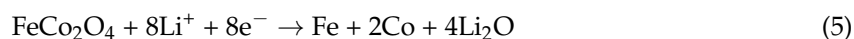
Figure 5. (a) X-ray diffraction (XRD) patterns of FeCo_2O_4 tubes on Ni foam before (black curve) and after MnO_2 covering (blue curve); (b) Scanning electron microscope (SEM) image of typical MnO_2 covered FeCo_2O_4 on Ni foam; (c) TEM image of an isolated MnO_2 covered FeCo_2O_4 tube; inset is the corresponding selected area electron diffraction (SAED) pattern recorded from a single tube; (1) and (2) label MnO_2 and FeCo_2O_4 , diffraction rings, respectively; (d) High-magnification TEM showing the MnO_2 nanosheets [28].

Combing different materials to form composites is also an important approach to improve the performance of supercapacitors. Some literatures reported FeCo_2O_4 and CoFe_2O_4 based composite materials served as supercapacitor electrodes. Zhu et al. [28], reported the MnO_2 -nanosheet covered sub micrometer FeCo_2O_4 -tube forest (Figure 5) as the high energy density supercapacitor electrode.

The deposition of MnO₂ nanosheets increased the specific capacitance to 3.3 F cm⁻² at 1 mA cm⁻², which doubled that of its bare FeCo₂O₄-tube electrode. Conducting polymers were promising as both excellent conductive substrates to junction to FeCo₂O₄ and CoFe₂O₄ and self-active pseudo-capacitance materials. For example, CoFe₂O₄/graphene/polyaniline nanocomposite was fabricated by the hydrothermal and in-situ polymerization processes. This ternary hybrid electrode exhibited a high capacitance of 1133.3 F g⁻¹ at a scan rate of 1 mV s⁻¹ and a 96% retention of the initial capacitance after 5000 cycles [27]. There were other reports on the enhancement of the specific capacitance and the cycling-stability of NiCo₂O₄ electrodes by combining carbon aerogel [37], polypyrrole [38] and transition metal oxides such as NiO [39]. This easily inspired the search for more alternative conductive juncture materials, such as rarely reported carbon nanotubes, graphene, polypyrrole and other transition metal oxides, to design and fabricate new novel FeCo₂O₄ and CoFe₂O₄ based composite electrodes.

3. Application for Lithium-Ion Batteries

Compared with supercapacitors, Lithium-ion battery possess a higher energy storage and high cell voltage but a lower power output. Its energy densities and power densities are twice and five times greater than those of the Pb-acid and the Ni-Cd batteries, respectively [40]. The further development of LIB is largely dependent on performance of its anode electrode materials. Graphite is a conventional commercial electrode material, only possessing a theoretical specific capacity at about 372 mA h g⁻¹ [41]. Transition metal oxides have been intensively explored as new promising anode materials because of their higher theoretical specific capacitances. For example, CoFe₂O₄ was reported to possess a high theoretical specific capacity at 914 mA h g⁻¹ for LIBs which was two times higher than that of graphite [42]. Considering the abundance on the earth and eco-friendliness of iron, iron cobalt oxides have been widely investigated as anode materials of LIBs. Previous literature reported that the electrochemical mechanisms of the Li-ions' storage of FeCo₂O₄ and CoFe₂O₄ obeyed the displaced redox reactions, demonstrated by the following equations.



Binary metal oxides electrode stored Li-ion mainly on both its interface to the electrolyte and its near-surface bulky structure. Figure 6 shows a schematic diagram of the LIB's charging-discharging process, in which, the electrode involves a reversible insertion and extraction of Li ions as described by above equations. The charging process is accomplished with Li ions extracted from the cathode and inserted into the anode and the discharging process is accomplished with Li ions deintercalated from the anode and intercalated into the cathode. The energy storage and release are realized by the intercalation and deintercalation of Li ions between the anode and cathode. However, there typically existed an irreversible capacity loss of FeCo₂O₄ and CoFe₂O₄ LIB starting from its first cycle due to the electrolyte-reduction induced incomplete conversion reaction and the formation of solid electrolyte interface (SEI) layer at the electrode/electrolyte interface [43]. The Li-ion insertion/extraction process also induced the large volume change, the severe aggregation and the low conductivity, resulting in the capacity degradation and the poor cycling stability [44,45].

Efforts have been devoted to remedy the aforementioned disadvantages of FeCo₂O₄ and CoFe₂O₄ electrodes in LIBs. This correlated their various morphologies and structures to different performance, as shown in Table 2. P. Lavela et al. [46], synthesized CoFe₂O₄ by way of the sol-gel process and Y.

Sharma et al. [47], synthesized FeCo_2O_4 by way of the urea combustion method, both confirming that the LIB performance of CoFe_2O_4 and FeCo_2O_4 were better than that of NiFe_2O_4 and MgCo_2O_4 , respectively. Different synthesis methods generated a broad and different dimensional morphologies of CoFe_2O_4 and FeCo_2O_4 materials. It has been found that the nanostructured iron cobalt oxides generally had higher reversible capacities and a more excellent rate capability than those of corresponding microstructured and bulky materials. The hollow-typed morphologies performed better than solid-typed morphologies in LIBs. Nanostructures provided higher surface areas which were favorable to reduce electron and lithium ions diffusion paths and increase active sites for lithium ion insertion/extraction [48,49]. Hollow-typed morphologies and structures can afford adequate spaces to relax the large volume changes during constant charge/discharge processes [50]. Both lead their excellent performance in LIBs. As typical examples, H. Guo et al. [51], fabricated hollow porous CoFe_2O_4 nanocubes via metal-organic frameworks and exhibited its excellent rate performance, as shown in Figure 7.

Table 2. Summary of previous bare iron cobalt oxides for Lithium-ion batteries applications.

Materials	Synthetic Method	Reversible Capacity (mA h g^{-1})	Rate Capability	Ref.
FeCo_2O_4 nanoflakes/NF	Hydrothermal	905 at 200 mA g^{-1} after 170 cycles	1222 mA h g^{-1} at 800 mA g^{-1}	[22]
3D ordered macroporous CoFe_2O_4	Templating	702 at 0.2 mA cm^{-2} after 30 cycles	816 mA h g^{-1} at 5 mA cm^{-2}	[42]
Hollow CoFe_2O_4 nanocubes	Metal-organic frameworks	1115 at 1 C after 200 cycles	815 mA h g^{-1} at 20 C	[51]
FeCo_2O_4 nanoneedles/NF	Hydrothermal	1129 at 100 mA g^{-1} after 350 cycles	875 mA h g^{-1} at 2 A g^{-1}	[52]
Hollow FeCo_2O_4 nanospheres	Soft-templating	1060 at 100 mA g^{-1} after 50 cycles	823 mA h g^{-1} at 1 A g^{-1}	[53]
FeCo_2O_4 octahedra	Evaporation-induced self-assembly	1101 at 1000 mA g^{-1} after 200 cycles	518 mA h g^{-1} at 10 A g^{-1}	[54]
CoFe_2O_4 nanosheets	Thermal decomposition	806 at 1 A g^{-1} after 200 cycles	303 mA h g^{-1} at 10 A g^{-1}	[55]
CoFe_2O_4 nanowires/FCF	Hydrothermal	954.3 at 200 mA g^{-1} after 150 cycles	$595.3 \text{ mA h g}^{-1}$ at 3.2 A g^{-1}	[56]
CoFe_2O_4 nanotubes	Self-templating	988 at 100 mA g^{-1} after 100 cycles	654 mA h g^{-1} at 5 A g^{-1}	[57]
Cubic aggregated CoFe_2O_4 nanoparticles	Hydrothermal	1133.5 at 100 mA g^{-1} after 120 cycles	679 mA h g^{-1} at 3.2 A g^{-1}	[58]
Layer-stacked CoFe_2O_4 platelets	Co-precipitation	580 at 5 A g^{-1} after 2000 cycles	654 mA h g^{-1} at 10 A g^{-1}	[59]
CoFe_2O_4 nanorods	Templating	800 at 1 A g^{-1} after 300 cycles	840 mA h g^{-1} at 1 A g^{-1}	[60]
CoFe_2O_4 octahedra	Sol-gel	992 at 100 mA g^{-1} after 200 cycles	366 mA h g^{-1} at 5 A g^{-1}	[61]
Hollow CoFe_2O_4 nanospheres	Hydrothermal	1185 at 90 mA g^{-1} after 50 cycles	1000 mA h g^{-1} at 900 mA g^{-1}	[62]
Flower-like CoFe_2O_4 microspheres	Hydrothermal	733.5 at 200 mA g^{-1} after 50 cycles	717 mA h g^{-1} at 1 A g^{-1}	[63]

NF: nickel foam; FCF: flexible carbon fabric.

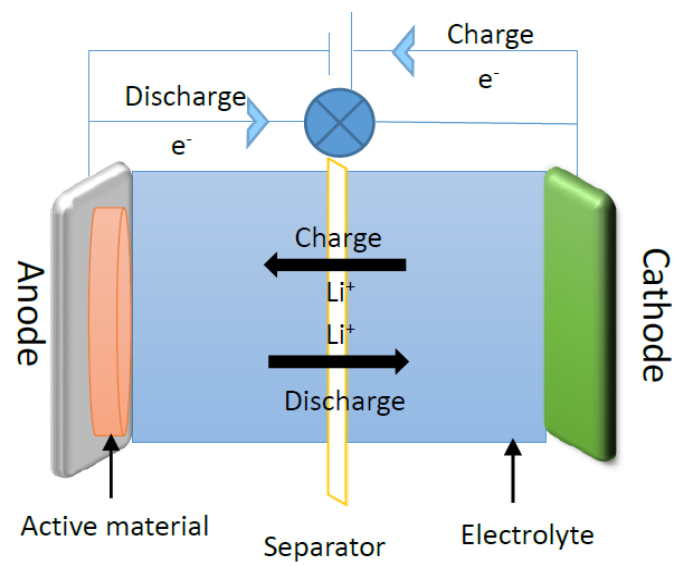


Figure 6. Schematic diagram of the charging-discharging process in Li-ion batteries.

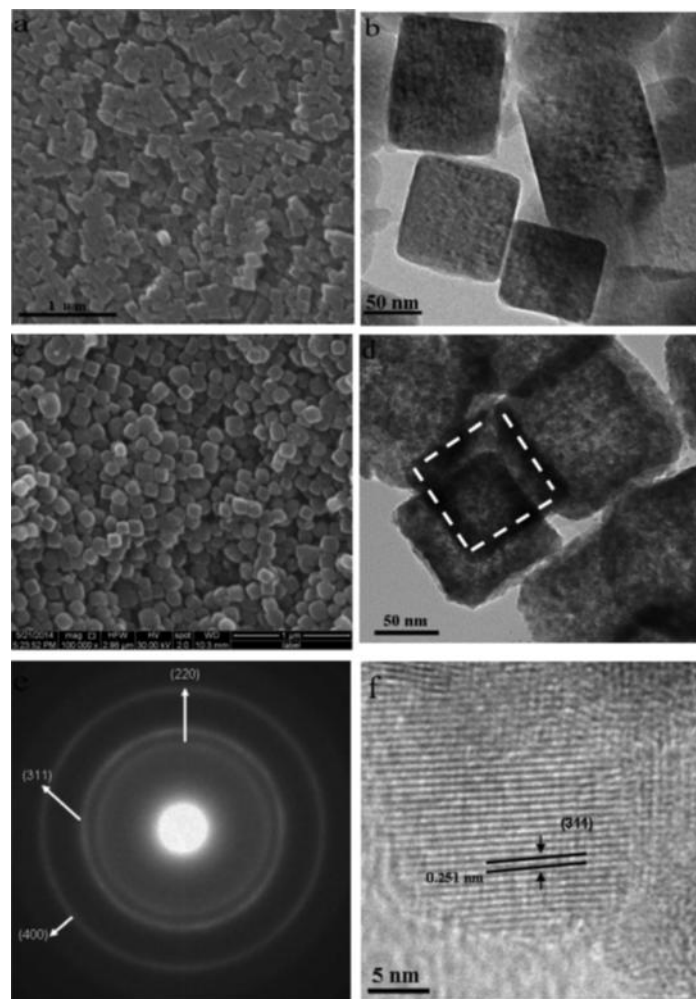


Figure 7. (a) SEM image and (b) TEM image of as prepared $\text{Co}[\text{Fe}(\text{CN})_6]_{0.667}$ nanocubes precursor; (c) SEM image, (d) TEM image, (e) SAED pattern and (f) High resolution transmission electron microscopy (HRTEM) image of as-synthesized hollow CoFe_2O_4 nanocubes [51].

Its surface area was $102.7 \text{ m}^2 \text{ g}^{-1}$ and its reversible capacity remained stable as high as 1115 mA h g^{-1} after 200 cycles at a constant current density of 1 C. Its capacity could reach 815 mA h g^{-1} even at a high current density of 20 C. Xiong et al. [63], developed an ascorbic acid-assisted hydrothermal method to prepare porous CoFe_2O_4 flower-like microspheres, and particles. The flower-like CoFe_2O_4 microsphere with the highest surface area of $51.0 \text{ m}^2 \text{ g}^{-1}$ showed a higher specific capacity of $733.5 \text{ mA h g}^{-1}$ at 200 mA g^{-1} after 50 cycles, contrasting to its microsphere counterpart of $616.7 \text{ mA h g}^{-1}$ with a surface area of $32.3 \text{ m}^2 \text{ g}^{-1}$ and its powder counterpart of $427.5 \text{ mA h g}^{-1}$ with a surface area of $15.1 \text{ m}^2 \text{ g}^{-1}$. Another recent binder/additive-free strategy was to directly grow CoFe_2O_4 and FeCo_2O_4 nanostructured materials on conductive substrates. Advantages of this approach were to enhance the electronic conductivity of electrodes, to provide a frame to organize nanostructured materials in order and to prevent the aggregation and pulverization of the electrode materials. Liu et al. [52], successfully synthesized a porous FeCo_2O_4 nanoneedles array on nickel foam (Figure 8) and confirmed the validity of this strategy. As shown in Figure 9a, the as-synthesized FeCo_2O_4 nanoneedles array exhibited a high rate capability of 875 mA h g^{-1} at 2 A g^{-1} , contrasting to bulky CoFe_2O_4 and FeCo_2O_4 nanoneedles array with 526 and 323 mA h g^{-1} at 2 A g^{-1} , respectively. It's found that the discharge capacity of FeCo_2O_4 nanoneedles array maintained at 1129 mA h g^{-1} with a capacity retention of 57.5%, while CoFe_2O_4 nanoneedles array dropped to 36.8% and bulky FeCo_2O_4 was only 19.3% (Figure 9b). Interestingly, we noticed that some reported $\text{FeCo}_2\text{O}_4/\text{CoFe}_2\text{O}_4$ based electrodes present much higher discharge capacity that their theoretical specific capacity. This higher discharge capacity should be attributed to an interfacial-storage mechanism, which was originated from the reversible formation–dissolution of an organic polymeric gel-like layer via electrolyte decomposition, inducing an extra capacity in the electrode material by way of the pseudocapacitive behavior [64].

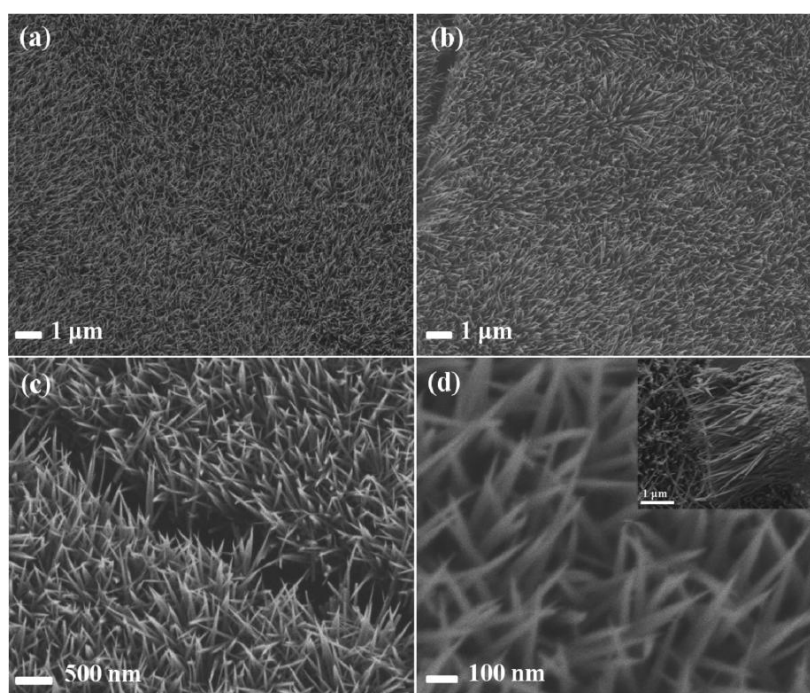


Figure 8. (a) SEM image of the (Fe, Co) bimetallic hydroxide carbonate precursors; (b–d) gradually magnified SEM images of FeCo_2O_4 nanoneedles array on nickel foam substrate. The inset of panel d displays the cross section of FeCo_2O_4 nanoneedles array exfoliation from nickel foam after a long time of powerful ultrasonic [52].

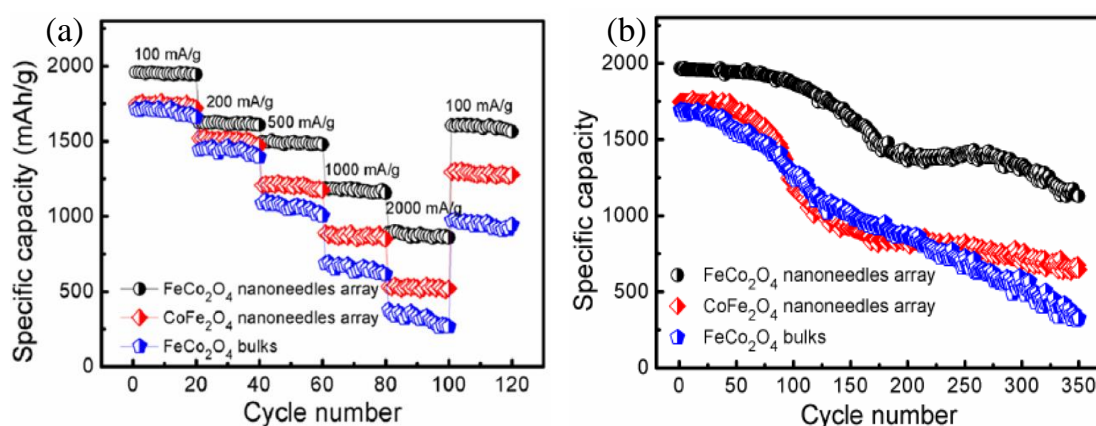


Figure 9. (a) Rate performance of FeCo₂O₄ nanoneedles array, CoFe₂O₄ nanoneedles array and FeCo₂O₄ bulks at various current densities; (b) Contrast experiment of cyclability for a FeCo₂O₄ nanoneedles array, a CoFe₂O₄ nanoneedles array and FeCo₂O₄ bulks [52].

Alternatively, the CoFe₂O₄ and FeCo₂O₄ based composite materials could also incorporate carbon materials, transition metal oxides and many other materials, dependent on if the incorporated material can enhance electrochemical performance of CoFe₂O₄ and FeCo₂O₄ in LIBs. It's found the proper morphologies and optimized ratio of incorporated components in composites were vital to well-performed electrodes via overcoming drawbacks of individual components and taking advantage of all constituents. Table 3 presents current iron cobalt oxides based composites for LIB applications. Carbon materials, such as carbon fibers, carbon nanotubes and graphene were typically used for synthesizing CoFe₂O₄ and FeCo₂O₄ based composite electrodes by virtue of their outstanding electrical conductivity, high surface areas and excellent mechanical and chemical stability [65]. Better electrical conductivity and higher surface area of iron cobalt oxides based materials could be further enhanced after their incorporation into porous carbon materials which could weaken the disadvantageous influence of polarization during the repeated discharge-charge process. Graphene was more favorable as an ideal component candidate toward the composite fabrication for LIBs, because of its conductive and accessible carbon open network to provide with sufficient growth sites for active materials and also prevent aggregation [66,67]. Wang et al. [68], immobilized CoFe₂O₄ nanoclusters on the aerogel-type graphene (Figure 10) via a facile one-step solvothermal method. The aerogel-type graphene clearly possessed an interconnected 3D framework, resulting in a high specific area, fast mass and electron transport rates and a unique nanostructure holding a large capacity of CoFe₂O₄ nanoclusters. As a result, the as-synthesized CoFe₂O₄ nanoclusters/graphene aerogels electrode exhibited 1070 mA h g⁻¹ at a current density of 100 mA g⁻¹ after 100 cycles, contrasting to only 473 mA h g⁻¹ of the bare CoFe₂O₄ electrode. It still possessed 221 mA h g⁻¹ at a high current density of 8 A g⁻¹. L. Wang et al. [69], also developed a green method to synthesize CoFe₂O₄ and graphene nanocomposite via a supercritical carbon dioxide. The uniform CoFe₂O₄ nanoparticles/graphene composite electrode exhibited a high reversible capacity of 1114 mA h g⁻¹ at a current density of 100 mA g⁻¹ after 100 cycles and an excellent rate capability of 636 mA h g⁻¹ at 3 A g⁻¹. Several reports on other components to be incorporated in CoFe₂O₄ addressed multiwalled carbon nanotubes [70], carbon nanofibers [71] and carbon nanoparticles [72] but were not competitive with graphene. This implied well-structured graphene was an optimal carbon material to be incorporated in iron cobalt oxides for the performance enhancement as electrode in LIBs.

Table 3. Summary of previous iron cobalt oxides based nanocomposites for Lithium-ion batteries applications.

Materials	Synthetic Method	Reversible Capacity (mA h g ⁻¹)	Rate Capability	Ref.
CoFe ₂ O ₄ nanoclusters/graphene aerogels	Solvothermal	966 at 500 mA g ⁻¹ after 300 cycles	221 mA h g ⁻¹ at 8 A g ⁻¹	[68]
CoFe ₂ O ₄ nanoparticles/graphene	Carbon dioxide-induced deposition	1114 at 100 mA g ⁻¹ after 100 cycles	636 mA h g ⁻¹ at 3 A g ⁻¹	[69]
Flower-like CoFe ₂ O ₄ /MWCNTs	Hydrothermal	823 at 45 mA g ⁻¹ after 50 cycles	359 mA h g ⁻¹ at 1.8 A g ⁻¹	[70]
CoFe ₂ O ₄ /carbon nanofibers	Pyrolysis-oxidation	705 at 100 mA g ⁻¹ after 250 cycles	-	[71]
CoFe ₂ O ₄ nanoparticles/Vulcan XC-72	Thermal decomposition	766 at 100 mA g ⁻¹ after 25 cycles	478 mA h g ⁻¹ at 1 C	[72]
C/CoFe ₂ O ₄ fiber-in-tube nanostructure	Electro-spinning	740 at 200 mA g ⁻¹ after 200 cycles	488 mA h g ⁻¹ at 1.6 A g ⁻¹	[73]
Core/shell structured CoFe ₂ O ₄ /onion-like C	Arc discharge	914.2 at 91.6 mA g ⁻¹ after 500 cycles	617.1 mA h g ⁻¹ at 916 mA g ⁻¹	[74]
CoFe ₂ O ₄ nanoclusters/RGO	Solvothermal	1040 at 91.4 mA g ⁻¹ after 30 cycles	380 mA h g ⁻¹ at 18.28 A g ⁻¹	[75]
CoFe ₂ O ₄ /graphene	Liquid-solid-solution assembly	1102 at 200 mA g ⁻¹ after 100 cycles	410 mA h g ⁻¹ at 6.4 A g ⁻¹	[76]
CoFe ₂ O ₄ /graphene nanocomposite	Hydrothermal	910 at 100 mA g ⁻¹ after 50 cycles	406 mA h g ⁻¹ at 2 A g ⁻¹	[77]
CoFe ₂ O ₄ /C twin elliptical frustums	One-pot refluxing reaction	875 at 500 mA g ⁻¹ after 600 cycles	631 mA h g ⁻¹ at 4 A g ⁻¹	[78]
CoFe ₂ O ₄ nanosheets/RGO	Solvent method	835.6 at 400 mA g ⁻¹ after 200 cycles	848.6 mA h g ⁻¹ at 1 A g ⁻¹	[79]
CoFe ₂ O ₄ /graphene sandwich	Solvothermal	1047 at 200 mA g ⁻¹ after 160 cycles	440 mA h g ⁻¹ at 1.6 A g ⁻¹	[80]
Co ₃ O ₄ /CoFe ₂ O ₄ nanocomposites	Auto combustion	896.4 at 64.1 mA g ⁻¹ after 60 cycles	328.1 mA h g ⁻¹ at 6 A g ⁻¹	[81]
CoO/CoFe ₂ O ₄ nanocomposites	Separate nucleation and aging	1040 at 100 mA g ⁻¹ after 30 cycles	490 mA h g ⁻¹ at 6.4 A g ⁻¹	[82]
CoO/CoFe ₂ O ₄ /N-doped graphene	Hydrothermal	1172 at 500 mA g ⁻¹ after 100 cycles	680 mA h g ⁻¹ at 2 A g ⁻¹	[83]
CoFe ₂ O ₄ /MnO ₂ /C nanotubes	Electrospinning and hydrothermal	713.6 at 100 mA g ⁻¹ after 250 cycles	310.6 mA h g ⁻¹ at 1 A g ⁻¹	[84]

RGO: reduced graphene oxide; MWCNT: multiwalled carbon nanotube.

Transition metal oxides have also been favorable candidates to be incorporated in iron cobalt oxides for the performance enhancement in of LIBs. Cobalt oxides, such as CoO and Co₃O₄, were two widely-investigated. The CoO [85] and Co₃O₄ [86] themselves were anode materials of LIBs with higher theoretical capacities at about 744 mA h g⁻¹ [87] and 890 mA h g⁻¹ [88], respectively. Previous report showed the hybridized bi-component transition metal oxides such as Co₃O₄ nanowire/MnO₂ core/shell nanocomposite had an improved energy storage performance over each individual component [89]. Some researchers further fabricated transition metal oxides/iron cobalt oxides composites as electrodes in LIBs. Rai et al. [81], reported Co₃O₄/CoFe₂O₄ nanocomposite with their ratio at 76.3:23.6% and found this electrode exhibited a higher reversible capacity about 1172 mA h g⁻¹ at 500 mA g⁻¹ after 100 cycles and also maintained a high rate capability of 328.1 mA h g⁻¹ at a current density of 6 A g⁻¹. Li et al. [82], fabricated CoO/CoFe₂O₄ nanocomposites via scalably prepared single-resource precursors of CoFe-layered double hydroxides. This CoO/CoFe₂O₄ composite showed the currently best performance with a capacity of 603 mA h g⁻¹ at a rate of 1000 mA g⁻¹ after 100 cycles and 490 mA h g⁻¹ at a high current density of 6.4 A g⁻¹. Its performances were much better than those of single CoO, CoFe₂O₄ and physical mixture of CoO and CoFe₂O₄. Results from composite

studies revealed the synergistic effects of incorporation of transition metal oxides in iron cobalt oxides for LIB applications. There were many reports on other transition metal oxides, such as NiO [90], ZnFe₂O₄ [91], MnO₂ [92], and SnO₂ [93], which exhibited their excellent performance in LIBs and implied their promising functionalities to be incorporated in iron cobalt oxides.

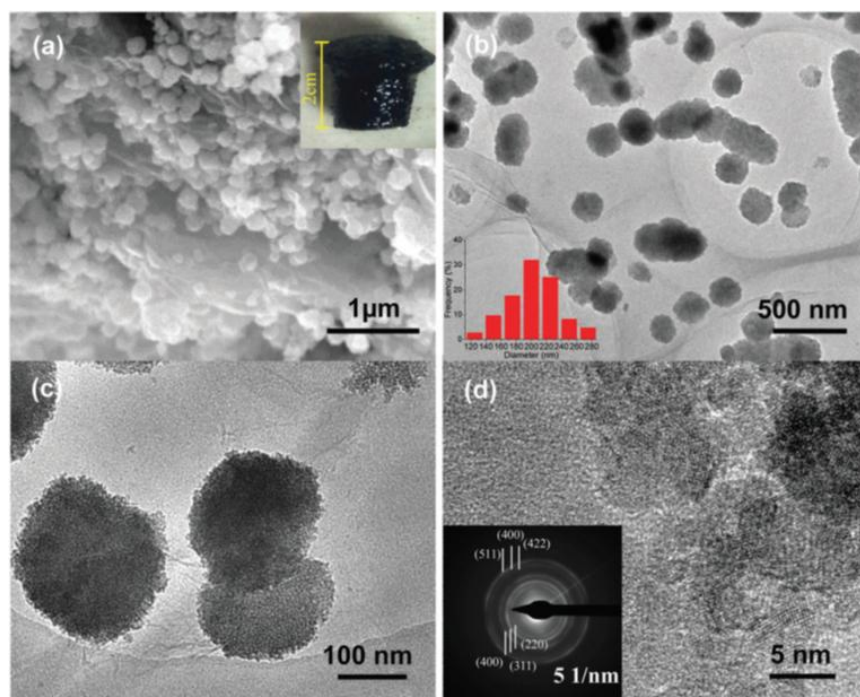


Figure 10. (a) SEM image of the CoFe₂O₄/GAs composite, (b–d) TEM and HRTEM images of CoFe₂O₄/GAs composite. Inset of (a) is a digital image of the resulting CoFe₂O₄/GAs composite. Inset of (b) is the diameter distribution of CoFe₂O₄. Inset of (d) is the corresponding SAED pattern of CoFe₂O₄ [68].

4. Application for Fuel Cells

Figure 1 has shown fuel cells can be electrochemical energy conversion devices with high energy density. Unlike supercapacitor and LIBs, fuel cells directly convert chemical energy of fuels into electricity in a highly efficiency. They involve combustion resulting in a highly efficient utilization of fuels. Different applied electrolytes categories fuel cells into five types, including Phosphoric Acid Fuel Cell (PAFC), Proton Exchange Membrane Fuel Cell (PEMFC), Alkaline Fuel Cell (AFC), Molten Carbonate Fuel Cell (MCFC) and Solid Oxide Fuel Cell (SOFC) [94]. Recent AFCs using potential non-noble catalysts have aroused more attention for achieving more efficient kinetics in both the oxygen reduction reaction (ORR) and methanol oxidation reaction (MOR) in alkaline system [95]. In alkaline electrolyte of AFC, oxygen can be reduced through either a four-electron process ($O_2 + 2H_2O + 4e^- \rightarrow 4OH^-$) or two two-electron processes ($O_2 + H_2O + 2e^- \rightarrow HO_2^- + OH^-$; $HO_2^- + H_2O + 2e^- \rightarrow 3 OH^-$) [96]. Noble metal materials such as Pt, [97] Pd, [98] Ru, [99] and Pt-based alloys [100] have long been considered as the most efficient catalysts for the ORR reaction in the past decades but its high cost restrains the commercialization of AFCs. Transitional metal oxide catalysts were such new group electrode materials for AFC to substitute the traditional noble metals in AFC applications.

Remarkably, CoFe₂O₄ and FeCo₂O₄ show excellent electrocatalytical activity for the ORR reaction in AFCs. Table 4 presents performance of current CoFe₂O₄ and FeCo₂O₄ based materials for the ORR reaction. Yang's group designed and fabricated several iron cobalt oxide nanostructures and nanocomposites, among which solid and hollow CoFe₂O₄ nanospheres were successfully fabricated [101]. Compared with the most efficient Pt/C, the hollow CoFe₂O₄ nanospheres showed

a negative shift of 180 mV at the half-wave potential, which is 40 mV more positive shift than the solid one, indicating that improved electrocatalytic activities were expected and also depended on the structures and morphologies of materials. When CoFe_2O_4 nanospheres were combined with graphene via a one-pot solvothermal method [102], their nanocomposite showed a low onset potential at about -0.11 V (vs. Ag/AgCl) which was higher than -0.17 for CoFe_2O_4 nanospheres only. The stability of CoFe_2O_4 nanospheres/graphene was also excellent in the ORR reaction, the ORR current density was still maintained at 94% after 72,000 s of continuous operation. The enhanced performance of CoFe_2O_4 nanospheres/graphene should be attributed to the suppressed agglomeration CoFe_2O_4 nanospheres and restacking of graphene as well as synergistic electrocatalytic effects of CoFe_2O_4 nanospheres and graphene in ORR reaction. The FeCo_2O_4 /hollow graphene spheres [103] (Figure 11) was the currently best performed CoFe_2O_4 and FeCo_2O_4 based nanocomposites, with an onset potential at about -0.09 V (vs. Ag/AgCl) which was very close to -0.01 V of the Pt/C electrode. Alternatively, FeCo_2O_4 /hollow graphene spheres exhibited high durability with 92.1% retention in the ORR current density over 86,400 s, contrasting to only 41.1% of the commercial Pt/C. The FeCo_2O_4 /hollow graphene spheres could be a substitutable low-cost and efficient material for the ORR process. Overall, the critical composite fabrication strategy is to select proper guest materials and optimize stoichiometric ratios and also control morphologies. This will call for novelties in both optimal morphology designs and proper material selections toward enhancing the electrocatalytic performance in the ORR reaction.

Table 4. Summary of previous cobalt iron oxides based materials for oxygen reduction reaction (ORR).

Materials	Synthetic Method	Onset Potential	Tafel Slope	Durability	Ref.
3D CoFe_2O_4 hollow nanospheres	Hydrothermal	0.78 V (vs. RHE)	-	34% decay after 43,200 s	[101]
Ni-doped CoFe_2O_4 hollow nanospheres	Hydrothermal	-0.15 V (vs. Ag/AgCl)	-	-	[104]
FeCo_2O_4 /hollow graphene spheres	Electrostatically induced assembly method	-0.09 V (vs. Ag/AgCl)	56 mV/dec	7.9% decay after 86,400 s	[103]
CoFe_2O_4 nanospheres/graphene	Solvothermal	-0.11 V (vs. Ag/AgCl)	61 mV/dec	6% decay after 72,000 s	[105]
CoFe_2O_4 /biocarbon nanocomposites	Biotemplate and chemical precipitation	-0.14 V (vs. Ag/AgCl)	-	15.1% decay after 43,000 s	[105]
CoFe_2O_4 /rod-like carbon	Hydrothermal	-0.1 V (vs. Ag/AgCl)	99 mV/dec	9.5% decay after 20,000 s	[106]
CoFe_2O_4 /Carbon nanotubes	Solvothermal	-0.124 V (vs. Ag/AgCl)	-	-	[107]
CoFe_2O_4 /graphene	Solvothermal	-0.136 V (vs. Ag/AgCl)	67 mV/dec	5.5% decay after 43,200 s	[108]
N,S dual-doped 3D RGO/ CoFe_2O_4	Hydrothermal	-0.14 V (vs. Ag/AgCl)	70 mV/dec	6.7% decay after 43,200 s	[109]
Ag/ CoFe_2O_4 /C	Solvothermal	$E_{1/2}$ at -0.13 V (vs. Hg/HgO)	-	5.2% decay after 5000 s	[110]
Co/CoO/ CoFe_2O_4 /graphene nanocomposites	Separate nucleation and aging	$E_{1/2}$ at -0.25 V (vs. Ag/AgCl)	-	20% decay after 20,000 s	[111]
MnO_2 - CoFe_2O_4 /C	Solvothermal	0.85 V (vs. RHE)	-	7.3% decay after 10,000 s	[112]

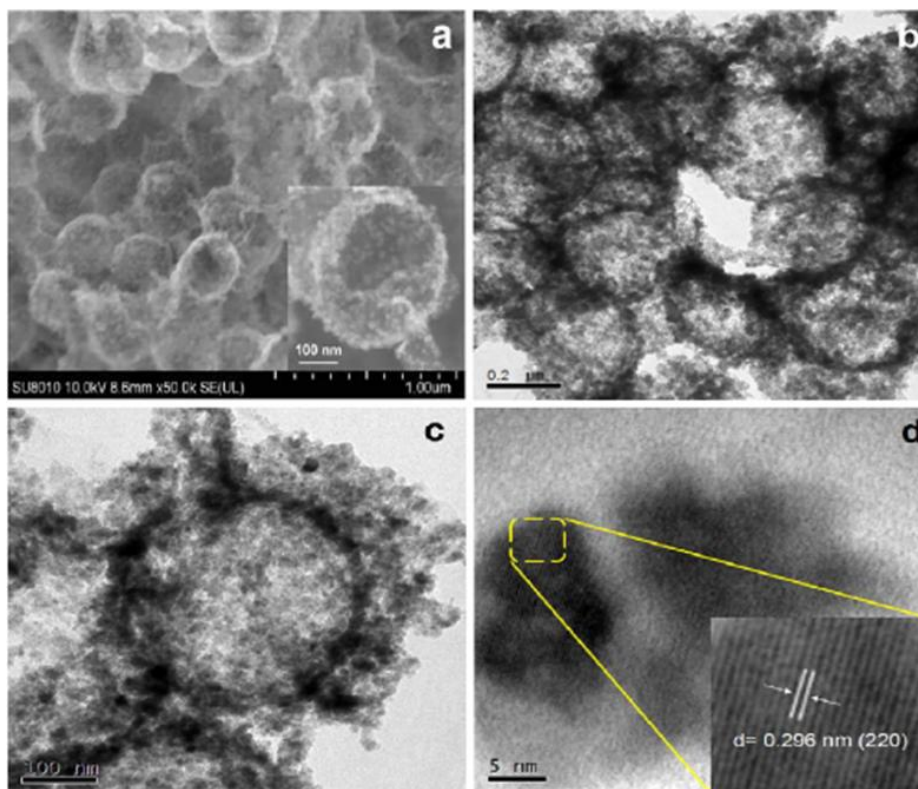


Figure 11. (a) SEM image of $\text{FeCo}_2\text{O}_4/\text{HrGOS}$; (b) and (c) TEM images of $\text{FeCo}_2\text{O}_4/\text{HrGOS}$ with different magnifications; (d) High resolution transmission electron microscopy (HRTEM) image of $\text{FeCo}_2\text{O}_4/\text{HrGOS}$ [103].

5. Summary and Outlook

In this review, we summarized recent advances in CoFe_2O_4 and FeCo_2O_4 based materials for energy storage and conversion applications, covering supercapacitors, Lithium-ion batteries and fuel cells. In order to realize better electrochemical performance, researchers have developed novel morphologies, structures and composites of CoFe_2O_4 and FeCo_2O_4 based materials. However, there was still some space to optimize performance of CoFe_2O_4 and FeCo_2O_4 based materials. Several recommendations were summarized as follows:

1. Previous studies identified the critical roles of morphologies and structures of electrode materials in enhancement of electrochemical performance. Novel structures were desired to be synthesized for further improving their electrochemical activities. It is noteworthy to mention that nanostructured materials should be focused considering their high specific areas and more active sites, 3D micron-structured or submicron-structured materials should also be addressed because of their excellent electrochemical performance.
2. More work focused on electrode materials, contrasting few works emphasized on electrolytes, separators and counter electrodes. The future works should oversee all involved components for the establishment of optimal systems to realize better performance.
3. More works emphasized on fabricating novel morphologies and structures, while few clearly addressed the essential mechanisms on charging-discharging process in energy storage and conversion. This missing correlation between morphologies and structures of CoFe_2O_4 and FeCo_2O_4 based materials has hampered their further optimization. The mechanical studies using DFT method was also highly recommended.

4. Current applied approaches to fabricate CoFe_2O_4 and FeCo_2O_4 based materials were limited to some classical methods such as hydrothermal, solvothermal and sol-gel. Those methods likely introduced impurities into electrode materials which later affected their performance to some extent. There was actually some space to refine the current methods but the development of new synthesis strategies of CoFe_2O_4 and FeCo_2O_4 based materials were highly demanding.
5. The scale-up preparation of CoFe_2O_4 and FeCo_2O_4 based materials was still challenging for their successful commercial applications. This was also true for other transition metal oxide electrode materials.
6. Many works only focused on the improvement of the basic electrochemical performance but missed the relevance toward their practical applications, such as adaptability to the load change and durability under severe working conditions. The current gap implied a long way ahead toward the commercialization.

Acknowledgments: This study was supported by the U.S. Department of Agriculture (5040-12630-004-00D), the 2017-2018 NSF EPSCoR program (the National Science Foundation under Cooperative Agreement No. 1355438) and the support from the NSF-CHE-MRI under the Award ID of 1338072. This work was also supported by grants from National Key Research and Development Plan of Intergovernmental International Scientific and Technological Innovation Cooperation (No. 2016YFE0108400) and the National Natural Science Foundation of China (No. 21676001).

Author Contributions: Hongyan Gao took care of the literature review and wrote this paper; Shuai Liu and Yafei Li sorted and compared the literature. Yan Cao coordinated this joint work and designed this paper. Eric Conte and Yan Cao supervised this paper writing.

Conflicts of Interest: The authors declare no conflict of interest.

References

1. Sharma, C.S.; Awasthi, R.; Singh, R.N.; Sinha, A.S.K. Graphene–cobaltite–Pd hybrid materials for use as efficient bifunctional electrocatalysts in alkaline direct methanol fuel cells. *Phys. Chem. Chem. Phys.* **2013**, *15*, 20333–20344. [[CrossRef](#)] [[PubMed](#)]
2. Zhao, X.; Johnston, C.; Grant, P.S. A novel hybrid supercapacitor with a carbon nanotube cathode and an iron oxide/carbon nanotube composite anode. *J. Mater. Chem.* **2009**, *19*, 8755–8760. [[CrossRef](#)]
3. Miller, J.R.; Simon, P. Electrochemical capacitors for energy management. *Sci. Mag.* **2008**, *321*, 651–652.
4. Spinner, N.; Mustain, W.E. Effect of nickel oxide synthesis conditions on its physical properties and electrocatalytic oxidation of methanol. *Electrochim. Acta* **2011**, *56*, 5656–5666. [[CrossRef](#)]
5. Winter, M.; Brodd, R.J. What are batteries, fuel cells, and supercapacitors? *Chem. Rev.* **2003**, *104*, 4245–4269. [[CrossRef](#)]
6. Liang, K.; Tang, X.; Hu, W. High-performance three-dimensional nanoporous NiO film as a supercapacitor electrode. *J. Mater. Chem.* **2012**, *22*, 11062–11067. [[CrossRef](#)]
7. Gao, Y.; Chen, S.; Cao, D.; Wang, G.; Yin, J. Electrochemical capacitance of Co_3O_4 nanowire arrays supported on nickel foam. *J. Power Sources* **2010**, *195*, 1757–1760. [[CrossRef](#)]
8. Cheng, K.; Cao, D.; Yang, F.; Xu, Y.; Sun, G.; Ye, K.; Yin, J.; Wang, G. Facile synthesis of morphology-controlled Co_3O_4 nanostructures through solvothermal method with enhanced catalytic activity for H_2O_2 electroreduction. *J. Power Sources* **2014**, *253*, 214–223. [[CrossRef](#)]
9. Yan, N.; Hu, L.; Li, Y.; Wang, Y.; Zhong, H.; Hu, X.; Kong, X.; Chen, Q. Co_3O_4 nanocages for high-performance anode material in lithium-ion batteries. *J. Phys. Chem. C* **2012**, *116*, 7227–7235. [[CrossRef](#)]
10. Chen, S.; Zhu, J.; Wu, X.; Han, Q.; Wang, X. Graphene oxide-MnO₂ nanocomposites for supercapacitors. *ACS NANO* **2010**, *4*, 2822–2830. [[CrossRef](#)] [[PubMed](#)]
11. He, Y.; Chen, W.; Li, X.; Zhang, Z.; Fu, J.; Zhao, C.; Xie, E. Freestanding three-dimensional graphene/MnO₂ composite networks as ultralight and flexible supercapacitor electrodes. *ACS NANO* **2012**, *7*, 174–182. [[CrossRef](#)] [[PubMed](#)]
12. Yu, M.; Chen, J.; Liu, J.; Li, S.; Ma, Y.; Zhang, J.; An, J. Mesoporous NiCo_2O_4 nanoneedles grown on 3D graphene-nickel foam for supercapacitor and methanol electro-oxidation. *Electrochim. Acta* **2015**, *151*, 99–108. [[CrossRef](#)]

13. Chen, Y.; Zhu, J.; Qu, B.; Lu, B.; Xu, Z. Graphene improving lithium-ion battery performance by construction of NiCo₂O₄/graphene hybrid nanosheet arrays. *Nano Energy* **2014**, *3*, 88–94. [[CrossRef](#)]
14. Kang, W.; Tang, Y.; Li, W.; Li, Z.; Yang, X.; Xu, J.; Lee, C.-S. Porous CuCo₂O₄ nanocubes wrapped by reduced graphene oxide as high-performance lithium-ion battery anodes. *Nanoscale* **2014**, *6*, 6551–6556. [[CrossRef](#)] [[PubMed](#)]
15. Simon, P.; Gogotsi, Y. Materials for electrochemical capacitors. *Nat. Mater.* **2008**, *7*, 845–854. [[CrossRef](#)] [[PubMed](#)]
16. Zhang, L.L.; Zhao, X.S. Carbon-based materials as supercapacitor electrodes. *Chem. Soc. Rev.* **2009**, *38*, 2520–2531. [[CrossRef](#)] [[PubMed](#)]
17. Wang, G.; Zhang, L.; Zhang, J. A review of electrode materials for electrochemical supercapacitors. *Chem. Soc. Rev.* **2012**, *41*, 797–828. [[CrossRef](#)] [[PubMed](#)]
18. Pendashteh, A.; Palma, J.; Anderson, M.; Marcilla, R. Nanostructured porous wires of iron cobaltite: Novel positive electrode for high-performance hybrid energy storage devices. *J. Mater. Chem. A* **2015**, *3*, 16849–16859. [[CrossRef](#)]
19. Lv, L.; Xu, Q.; Ding, R.; Qi, L.; Wang, H. Chemical synthesis of mesoporous CoFe₂O₄ nanoparticles as promising bifunctional electrode materials for supercapacitors. *Mater. Lett.* **2013**, *111*, 35–38. [[CrossRef](#)]
20. Wang, Z.; Jia, W.; Jiang, M.; Chen, C.; Li, Y. One-step accurate synthesis of shell controllable CoFe₂O₄ hollow microspheres as high-performance electrode materials in supercapacitor. *Nano Res.* **2016**, *9*, 2026–2033. [[CrossRef](#)]
21. Kumbhar, V.S.; Jagdale, A.D.; Shinde, N.M.; Lokhande, C.D. Chemical synthesis of spinel cobalt ferrite (CoFe₂O₄) nano-flakes for supercapacitor application. *Appl. Surf. Sci.* **2012**, *259*, 39–43. [[CrossRef](#)]
22. Mohamed, S.G.; Chen, C.-J.; Chen, C.K.; Hu, S.-F.; Liu, R.-S. High-performance lithium-ion battery and symmetric supercapacitors based on FeCo₂O₄ nanoflakes electrodes. *ACS Appl. Mater. Interfaces* **2014**, *6*, 22701–22708. [[CrossRef](#)] [[PubMed](#)]
23. Gao, H.; Xiang, J.; Cao, Y. Hierarchically porous CoFe₂O₄ nanosheets supported on Ni foam with excellent electrochemical properties for asymmetric supercapacitors. *Appl. Surf. Sci.* **2017**, *413*, 351–359. [[CrossRef](#)]
24. Liu, L.; Zhang, H.; Mu, Y.; Bai, Y.; Wang, Y. Binary cobalt ferrite nanomesh arrays as the advanced binder-free electrode for applications in oxygen evolution reaction and supercapacitors. *J. Power Sources* **2016**, *327*, 599–609. [[CrossRef](#)]
25. Zhu, B.; Tang, S.; Vongehr, S.; Xie, H.; Zhu, J.; Meng, X. FeCo₂O₄ submicron-tube arrays grown on Ni foam as high rate-capability and cycling-stability electrodes allowing superior energy and power densities with symmetric supercapacitors. *Chem. Commun.* **2016**, *52*, 2624–2627. [[CrossRef](#)] [[PubMed](#)]
26. Sankar, K.V.; Selvan, R.K.; Meyrick, D. Electrochemical performances of CoFe₂O₄ nanoparticles and a rGO based asymmetric supercapacitor. *RSC Adv.* **2015**, *5*, 99959–99967. [[CrossRef](#)]
27. Xiong, P.; Huang, H.; Wang, X. Design and synthesis of ternary cobalt ferrite/graphene/polyaniline hierarchical nanocomposites for high-performance supercapacitors. *J. Power Sources* **2014**, *245*, 937–946. [[CrossRef](#)]
28. Zhu, B.; Tang, S.; Vongehr, S.; Xie, H.; Meng, X. Hierarchically MnO₂-nanosheet covered submicrometer-FeCo₂O₄-tube forest as binder-free electrodes for high energy density all-solid-state supercapacitors. *ACS Appl. Mater. Interfaces* **2016**, *8*, 4762–4770. [[CrossRef](#)] [[PubMed](#)]
29. Gao, H.; Cao, S.; Cao, Y. Hierarchical Core-Shell Nanosheet Arrays with MnO₂ Grown on Mesoporous CoFe₂O₄ Support for High-Performance Asymmetric Supercapacitors. *Electrochim. Acta* **2017**, *240*, 31–42. [[CrossRef](#)]
30. Lin, L.; Tang, S.; Zhao, S.; Peng, X.; Hu, N. Hierarchical three-dimensional FeCo₂O₄@MnO₂ core-shell nanosheet arrays on nickel foam for high-performance supercapacitor. *Electrochim. Acta* **2017**, *228*, 175–182. [[CrossRef](#)]
31. Zhang, Y.X.; Hao, X.D.; Diao, Z.P.; Li, J.; Guan, Y.M. One-pot controllable synthesis of flower-like CoFe₂O₄/FeOOH nanocomposites for high-performance supercapacitors. *Mater. Lett.* **2014**, *123*, 229–234. [[CrossRef](#)]
32. Sankar, K.V.; Selvan, R.K. Fabrication of flexible fiber supercapacitor using covalently grafted CoFe₂O₄/reduced graphene oxide/polyaniline and its electrochemical performances. *Electrochim. Acta* **2016**, *213*, 469–481. [[CrossRef](#)]

33. Wang, Q.; Wang, X.; Liu, B.; Yu, G.; Hou, X.; Chen, D.; Shen, G. NiCo₂O₄ nanowire arrays supported on Ni foam for high-performance flexible all-solid-state supercapacitors. *J. Mater. Chem. A* **2013**, *1*, 2468–2473. [[CrossRef](#)]
34. Yuan, C.; Li, J.; Hou, L.; Zhang, X.; Shen, L.; Lou, X.W.D. Ultrathin mesoporous NiCo₂O₄ nanosheets supported on Ni foam as advanced electrodes for supercapacitors. *Adv. Funct. Mater.* **2012**, *22*, 4592–4597. [[CrossRef](#)]
35. Liu, S.; Hui, K.S.; Hui, K.N. Flower-like copper cobaltite nanosheets on graphite paper as high-performance supercapacitor electrodes and enzymeless glucose sensors. *ACS Appl. Mater. Interfaces* **2016**, *8*, 3258–3267. [[CrossRef](#)] [[PubMed](#)]
36. Bao, F.; Wang, X.; Zhao, X.; Wang, Y.; Ji, Y.; Zhang, H.; Liu, X. Controlled growth of mesoporous ZnCo₂O₄ nanosheet arrays on Ni foam as high-rate electrodes for supercapacitors. *RSC Adv.* **2014**, *4*, 2393–2397. [[CrossRef](#)]
37. Chien, H.C.; Cheng, W.Y.; Wang, Y.H.; Lu, S.Y. Ultrahigh specific capacitances for supercapacitors achieved by nickel cobaltite/carbon aerogel composites. *Adv. Funct. Mater.* **2012**, *22*, 5038–5043. [[CrossRef](#)]
38. Xu, K.; Huang, X.; Liu, Q.; Zou, R.; Li, W.; Liu, X.; Li, S.; Yang, J.; Hu, J. Understanding the effect of polypyrrole and poly(3,4-ethylenedioxythiophene) on enhancing the supercapacitor performance of NiCo₂O₄ electrodes. *J. Mater. Chem. A* **2014**, *2*, 16731–16739. [[CrossRef](#)]
39. Yang, W.; Gao, Z.; Ma, J.; Zhang, X.; Wang, J.; Liu, J. Hierarchical NiCo₂O₄@ NiO core-shell hetero-structured nanowire arrays on carbon cloth for a high-performance flexible all-solid-state electrochemical capacitor. *J. Mater. Chem. A* **2014**, *2*, 1448–1457. [[CrossRef](#)]
40. Ji, L.; Rao, M.; Aloni, S.; Wang, L.; Cairns, E.J.; Zhang, Y. Porous carbon nanofiber-sulfur composite electrodes for lithium/sulfur cells. *Energy Environ. Sci.* **2011**, *4*, 5053–5059. [[CrossRef](#)]
41. Tarascon, J.M.; Armand, M. Issues and challenges facing rechargeable lithium batteries. *Nature* **2001**, *414*, 359–367. [[CrossRef](#)] [[PubMed](#)]
42. Li, Z.H.; Zhao, T.P.; Zhan, X.Y.; Gao, D.S.; Xiao, Q.Z.; Lei, G.T. High capacity three-dimensional ordered macroporous CoFe₂O₄ as anode material for lithium ion batteries. *Electrochim. Acta* **2010**, *55*, 4594–4598. [[CrossRef](#)]
43. Zhou, G.; Wang, D.-W.; Li, F.; Zhang, L.; Li, N.; Wu, Z.-S.; Wen, L.; Lu, G.Q.; Cheng, H.-M. Graphene-wrapped Fe₃O₄ anode material with improved reversible capacity and cyclic stability for lithium ion batteries. *Chem. Mater.* **2010**, *22*, 5306–5313. [[CrossRef](#)]
44. Cabana, J.; Monconduit, L.; Larcher, D.; Palacin, M.R. Beyond Intercalation-Based Li-Ion Batteries: The State of the Art and Challenges of Electrode Materials Reacting Through Conversion Reactions. *Adv. Mater.* **2010**, *22*. [[CrossRef](#)]
45. Li, S.; Wang, B.; Liu, J.; Yu, M. In situ one-step synthesis of CoFe₂O₄/graphene nanocomposites as high-performance anode for lithium-ion batteries. *Electrochim. Acta* **2014**, *129*, 33–39. [[CrossRef](#)]
46. Lavela, P.; Tirado, J.L. CoFe₂O₄ and NiFe₂O₄ synthesized by sol-gel procedures for their use as anode materials for Li ion batteries. *J. Power Sources* **2007**, *172*, 379–387. [[CrossRef](#)]
47. Sharma, Y.; Sharma, N.; Rao, G.V.S.; Chowdari, B.V.R. Studies on spinel cobaltites, FeCo₂O₄ and MgCo₂O₄ as anodes for Li-ion batteries. *Solid State Ion.* **2008**, *179*, 587–597. [[CrossRef](#)]
48. Nam, K.T.; Kim, D.-W.; Yoo, P.J.; Chiang, C.-Y.; Meethong, N.; Hammond, P.T.; Chiang, Y.-M.; Belcher, A.M. Virus-enabled synthesis and assembly of nanowires for lithium ion battery electrodes. *Science* **2006**, *312*, 885–888. [[CrossRef](#)] [[PubMed](#)]
49. Lou, X.W.; Deng, D.; Lee, J.Y.; Feng, J.; Archer, L.A. Self-supported formation of needlelike Co₃O₄ nanotubes and their application as lithium-ion battery electrodes. *Adv. Mater.* **2008**, *20*, 258–262. [[CrossRef](#)]
50. Shi, Y.; Guo, B.; Corr, S.A.; Shi, Q.; Hu, Y.-S.; Heier, K.R.; Chen, L.; Seshadri, R.; Stucky, G.D. Ordered mesoporous metallic MoO₂ materials with highly reversible lithium storage capacity. *Nano Lett.* **2009**, *9*, 4215–4220. [[CrossRef](#)] [[PubMed](#)]
51. Guo, H.; Li, T.; Chen, W.; Liu, L.; Yang, X.; Wang, Y.; Guo, Y. General design of hollow porous CoFe₂O₄ nanocubes from metal-organic frameworks with extraordinary lithium storage. *Nanoscale* **2014**, *6*, 15168–15174. [[CrossRef](#)] [[PubMed](#)]
52. Liu, L.; Zhang, H.; Mu, Y.; Yang, J.; Wang, Y. Porous iron cobaltate nanoneedles array on nickel foam as anode materials for lithium-ion batteries with enhanced electrochemical performance. *ACS Appl. Mater. Interfaces* **2016**, *8*, 1351–1359. [[CrossRef](#)] [[PubMed](#)]

53. Liu, L.; Hu, Z.; Sun, L.; Gao, G.; Liu, X. Controlled synthesis and enhanced electrochemical performance of Prussian blue analogue-derived hollow FeCo_2O_4 nanospheres as lithium-ion battery anodes. *RSC Adv.* **2015**, *5*, 36575–36581. [[CrossRef](#)]
54. Zhu, H.; Sun, Y.; Zhang, X.; Tang, L.; Guo, J. Evaporation-induced self-assembly synthesis of mesoporous FeCo_2O_4 octahedra with large and fast lithium storage properties. *Mater. Lett.* **2016**, *166*, 1–4. [[CrossRef](#)]
55. Yao, X.; Kong, J.; Tang, X.; Zhou, D.; Zhao, C.; Zhou, R.; Lu, X. Facile synthesis of porous CoFe_2O_4 nanosheets for lithium-ion battery anodes with enhanced rate capability and cycling stability. *RSC Adv.* **2014**, *4*, 27488–27492. [[CrossRef](#)]
56. Wang, B.; Li, S.; Wu, X.; Li, B.; Liu, J.; Yu, M. Nanocrystal-constructed mesoporous CoFe_2O_4 nanowire arrays aligned on flexible carbon fabric as integrated anodes with enhanced lithium storage properties. *Phys. Chem. Chem. Phys.* **2015**, *17*, 21476–21484. [[CrossRef](#)] [[PubMed](#)]
57. Zhang, X.; Xie, Y.; Sun, Y.; Zhang, Q.; Zhu, Q.; Hou, D.; Guo, J. Self-template synthesis of CoFe_2O_4 nanotubes for high-performance lithium storage. *RSC Adv.* **2015**, *5*, 29837–29841. [[CrossRef](#)]
58. Mao, J.; Hou, X.; Wang, X.; Hu, S.; Xiang, L. The cubic aggregated CoFe_2O_4 nanoparticle anode material for lithium ion battery with good performance. *Mater. Lett.* **2015**, *161*, 652–655. [[CrossRef](#)]
59. Zhang, Z.; Li, W.; Zou, R.; Kang, W.; San Chui, Y.; Yuen, M.F.; Lee, C.-S.; Zhang, W. Layer-stacked cobalt ferrite (CoFe_2O_4) mesoporous platelets for high-performance lithium ion battery anodes. *J. Mater. Chem. A* **2015**, *3*, 6990–6997. [[CrossRef](#)]
60. Wang, N.; Xu, H.; Chen, L.; Gu, X.; Yang, J.; Qian, Y. A general approach for MFe_2O_4 ($\text{M} = \text{Zn}, \text{Co}, \text{Ni}$) nanorods and their high performance as anode materials for lithium ion batteries. *J. Power Sources* **2014**, *247*, 163–169. [[CrossRef](#)]
61. Guo, J.; Zhang, X.; Sun, Y.; Zhang, X. Mesoporous CoFe_2O_4 octahedra with high-capacity and long-life lithium storage properties. *RSC Adv.* **2016**, *6*, 18–22. [[CrossRef](#)]
62. Wang, Y.; Su, D.; Ung, A.; Ahn, J.-H.; Wang, G. Hollow CoFe_2O_4 nanospheres as a high capacity anode material for lithium ion batteries. *Nanotechnology* **2012**, *23*, 055402. [[CrossRef](#)] [[PubMed](#)]
63. Xiong, Q.Q.; Tu, J.P.; Shi, S.J.; Liu, X.Y.; Wang, X.L.; Gu, C.D. Ascorbic acid-assisted synthesis of cobalt ferrite (CoFe_2O_4) hierarchical flower-like microspheres with enhanced lithium storage properties. *J. Power Sources* **2014**, *256*, 153–159. [[CrossRef](#)]
64. Yuvaraj, S.; Selvan, R.K.; Lee, Y.S. An overview of AB_2O_4 - and A_2BO_4 -structured negative electrodes for advanced Li-ion batteries. *RSC Adv.* **2016**, *6*, 21448–21474. [[CrossRef](#)]
65. Liu, C.; Li, F.; Ma, L.P.; Cheng, H.M. Advanced materials for energy storage. *Adv. Mater.* **2010**, *22*. [[CrossRef](#)] [[PubMed](#)]
66. Qiu, B.; Xing, M.; Zhang, J. Mesoporous TiO_2 nanocrystals grown in situ on graphene aerogels for high photocatalysis and lithium-ion batteries. *J. Am. Chem. Soc.* **2014**, *136*, 5852–5855. [[CrossRef](#)] [[PubMed](#)]
67. Wu, Z.-S.; Ren, W.; Wen, L.; Gao, L.; Zhao, J.; Chen, Z.; Zhou, G.; Li, F.; Cheng, H.-M. Graphene anchored with Co_3O_4 nanoparticles as anode of lithium ion batteries with enhanced reversible capacity and cyclic performance. *ACS NANO* **2010**, *4*, 3187–3194. [[CrossRef](#)] [[PubMed](#)]
68. Wang, B.; Wang, G.; Lv, Z.; Wang, H. In situ synthesis of hierarchical CoFe_2O_4 nanoclusters/graphene aerogels and their high performance for lithium-ion batteries. *Phys. Chem. Chem. Phys.* **2015**, *17*, 27109–27117. [[CrossRef](#)] [[PubMed](#)]
69. Wang, L.; Zhuo, L.; Zhang, C.; Zhao, F. Carbon dioxide-induced homogeneous deposition of nanometer-sized cobalt ferrite (CoFe_2O_4) on graphene as high-rate and cycle-stable anode materials for lithium-ion batteries. *J. Power Sources* **2015**, *275*, 650–659. [[CrossRef](#)]
70. Wang, Y.; Park, J.; Sun, B.; Ahn, H.; Wang, G. Wintersweet-Flower-Like CoFe_2O_4 /MWCNTs Hybrid Material for High-Capacity Reversible Lithium Storage. *Chem. Asian J.* **2012**, *7*, 1940–1946. [[CrossRef](#)] [[PubMed](#)]
71. Ren, S.; Zhao, X.; Chen, R.; Fichtner, M. A facile synthesis of encapsulated CoFe_2O_4 into carbon nanofibres and its application as conversion anodes for lithium ion batteries. *J. Power Sources* **2014**, *260*, 205–210. [[CrossRef](#)]
72. Sener, T.; Kayhan, E.; Sevim, M.; Metin, O. Monodisperse CoFe_2O_4 nanoparticles supported on Vulcan XC-72: High performance electrode materials for lithium-air and lithium-ion batteries. *J. Power Sources* **2015**, *288*, 36–41. [[CrossRef](#)]

73. Wang, J.; Yang, G.; Wang, L.; Yan, W.; Wei, W. C@CoFe₂O₄ fiber-in-tube mesoporous nanostructure: Formation mechanism and high electrochemical performance as an anode for lithium-ion batteries. *J. Alloy. Compd.* **2017**, *693*, 110–117. [[CrossRef](#)]
74. Liu, X.; Wu, N.; Cui, C.; Zhou, P.; Sun, Y. Enhanced rate capability and cycling stability of core/shell structured CoFe₂O₄/onion-like C nanocapsules for lithium-ion battery anodes. *J. Alloy. Compd.* **2015**, *644*, 59–65. [[CrossRef](#)]
75. Kumar, P.R.; Kollu, P.; Santhosh, C.; Rao, K.E.V.; Kim, D.K.; Grace, A.N. Enhanced properties of porous CoFe₂O₄-reduced graphene oxide composites with alginate binders for Li-ion battery applications. *New J. Chem.* **2014**, *38*, 3654–3661. [[CrossRef](#)]
76. Zhu, Y.; Lv, X.; Zhang, L.; Guo, X.; Liu, D.; Chen, J.; Ji, J. Liquid-Solid-Solution Assembly of CoFe₂O₄/Graphene Nanocomposite as a High-Performance Lithium-Ion Battery Anode. *Electrochim. Acta* **2016**, *215*, 247–252. [[CrossRef](#)]
77. Xia, H.; Zhu, D.; Fu, Y.; Wang, X. CoFe₂O₄-graphene nanocomposite as a high-capacity anode material for lithium-ion batteries. *Electrochim. Acta* **2012**, *83*, 166–174. [[CrossRef](#)]
78. Xiang, Y.; Wu, H.; Zhang, K.H.L.; Coto, M.; Zhao, T.; Chen, S.; Dong, B.; Lu, S.; Abdelkader, A.; Guo, Y. Quick one-pot synthesis of amorphous carbon-coated cobalt-ferrite twin elliptical frustums for enhanced lithium storage capability. *J. Mater. Chem. A* **2017**, *5*, 8062–8069. [[CrossRef](#)]
79. Dong, B.; Li, M.; Xiao, C.; Ding, D.; Gao, G.; Ding, S. Tunable growth of perpendicular cobalt ferrite nanosheets on reduced graphene oxide for energy storage. *Nanotechnology* **2016**, *28*, 055401. [[CrossRef](#)] [[PubMed](#)]
80. Liu, S.; Xie, J.; Fang, C.; Cao, G.; Zhu, T.; Zhao, X. Self-assembly of a CoFe₂O₄/graphene sandwich by a controllable and general route: Towards a high-performance anode for Li-ion batteries. *J. Mater. Chem.* **2012**, *22*, 19738–19743. [[CrossRef](#)]
81. Rai, A.K.; Gim, J.; Thi, T.V.; Ahn, D.; Cho, S.J.; Kim, J. High rate capability and long cycle stability of Co₃O₄/CoFe₂O₄ nanocomposite as an anode material for high-performance secondary lithium ion batteries. *J. Phys. Chem. C* **2014**, *118*, 11234–11243. [[CrossRef](#)]
82. Li, M.; Yin, Y.-X.; Li, C.; Zhang, F.; Wan, L.-J.; Xu, S.; Evans, D.G. Well-dispersed bi-component-active CoO/CoFe₂O₄ nanocomposites with tunable performances as anode materials for lithium-ion batteries. *Chem. Commun.* **2012**, *48*, 410–412. [[CrossRef](#)] [[PubMed](#)]
83. Zhao, C.; Yu, C.; Liu, S.; Yang, J.; Fan, X.; Qiu, J. Facile Fabrication of Bicomponent CoO/CoFe₂O₄-N-Doped Graphene Hybrids with Ultrahigh Lithium Storage Capacity. *Part. Part. Syst. Charact.* **2015**, *32*, 91–97. [[CrossRef](#)]
84. Zhou, J.; Yang, T.; Mao, M.; Ren, W.; Li, Q. Enhanced electrochemical performance of hierarchical CoFe₂O₄/MnO₂/C nanotubes as anode materials for lithium-ion batteries. *J. Mater. Chem. A* **2015**, *3*, 12328–12333. [[CrossRef](#)]
85. Guan, H.; Wang, X.; Li, H.; Zhi, C.; Zhai, T.; Bando, Y.; Golberg, D. CoO octahedral nanocages for high-performance lithium ion batteries. *Chem. Commun.* **2012**, *48*, 4878–4880. [[CrossRef](#)] [[PubMed](#)]
86. Li, Y.; Tan, B.; Wu, Y. Mesoporous Co₃O₄ nanowire arrays for lithium ion batteries with high capacity and rate capability. *Nano Lett.* **2008**, *8*, 265–270. [[CrossRef](#)] [[PubMed](#)]
87. Wang, X.; Fu, H.; Peng, A.; Zhai, T.; Ma, Y.; Yuan, F.; Yao, J. One-Pot Solution Synthesis of Cubic Cobalt Nanoskeletons. *Adv. Mater.* **2009**, *21*, 1636–1640. [[CrossRef](#)]
88. Poizot, P.; Laruelle, S.; Grugeon, S.; Dupont, L.; Tarascon, J.M. Nano-sized transition-metal oxides as negative-electrode materials for lithium-ion batteries. *Nature* **2000**, *407*, 496. [[CrossRef](#)] [[PubMed](#)]
89. Liu, J.; Jiang, J.; Cheng, C.; Li, H.; Zhang, J.; Gong, H.; Fan, H.J. Co₃O₄ Nanowire@MnO₂ Ultrathin Nanosheet Core/Shell Arrays: A New Class of High-Performance Pseudocapacitive Materials. *Adv. Mater.* **2011**, *23*, 2076–2081. [[CrossRef](#)] [[PubMed](#)]
90. Liu, H.; Wang, G.; Liu, J.; Qiao, S.; Ahn, H. Highly ordered mesoporous NiO anode material for lithium ion batteries with an excellent electrochemical performance. *J. Mater. Chem.* **2011**, *21*, 3046–3052. [[CrossRef](#)]
91. Teh, P.F.; Sharma, Y.; Pramana, S.S.; Srinivasan, M. Nanoweb anodes composed of one-dimensional, high aspect ratio, size tunable electrospun ZnFe₂O₄ nanofibers for lithium ion batteries. *J. Mater. Chem.* **2011**, *21*, 14999–15008. [[CrossRef](#)]
92. Guo, X.; Han, J.; Zhang, L.; Liu, P.; Hirata, A.; Chen, L.; Fujita, T.; Chen, M. A nanoporous metal recuperated MnO₂ anode for lithium ion batteries. *Nanoscale* **2015**, *7*, 15111–15116. [[CrossRef](#)] [[PubMed](#)]

93. Liu, X.; Zhang, J.; Si, W.; Xi, L.; Oswald, S.; Yan, C.; Schmidt, O.G. High-rate amorphous SnO₂ nanomembrane anodes for Li-ion batteries with a long cycling life. *Nanoscale* **2015**, *7*, 282–288. [[CrossRef](#)] [[PubMed](#)]
94. Kirubakaran, A.; Jain, S.; Nema, R.K. A review on fuel cell technologies and power electronic interface. *Renew. Sustain. Energy Rev.* **2009**, *13*, 2430–2440. [[CrossRef](#)]
95. Li, Y.S.; Zhao, T.S.; Liang, Z.X. Effect of polymer binders in anode catalyst layer on performance of alkaline direct ethanol fuel cells. *J. Power Sources* **2009**, *190*, 223–229. [[CrossRef](#)]
96. Zheng, Y.; Jiao, Y.; Jaroniec, M.; Jin, Y.; Qiao, S.Z. Nanostructured Metal-Free Electrochemical Catalysts for Highly Efficient Oxygen Reduction. *Small* **2012**, *8*, 3550–3566. [[CrossRef](#)] [[PubMed](#)]
97. Gu, L.; Luo, N.; Miley, G.H. Cathode electrocatalyst selection and deposition for a direct borohydride/hydrogen peroxide fuel cell. *J. Power Sources* **2007**, *173*, 77–85. [[CrossRef](#)]
98. Wang, H.; Sun, Z.; Yang, Y.; Su, D. The growth and enhanced catalytic performance of Au@Pd core-shell nanodendrites. *Nanoscale* **2013**, *5*, 139–142. [[CrossRef](#)] [[PubMed](#)]
99. Kua, J.; Goddard, W.A. Oxidation of methanol on 2nd and 3rd row group VIII transition metals (Pt, Ir, Os, Pd, Rh, and Ru): Application to direct methanol fuel cells. *J. Am. Chem. Soc.* **1999**, *121*, 10928–10941. [[CrossRef](#)]
100. Xia, B.Y.; Wu, H.B.; Wang, X.; Lou, X.W. One-pot synthesis of cubic PtCu₃ nanocages with enhanced electrocatalytic activity for the methanol oxidation reaction. *J. Am. Chem. Soc.* **2012**, *134*, 13934–13937. [[CrossRef](#)] [[PubMed](#)]
101. Xu, Y.; Bian, W.; Wu, J.; Tian, J.-H.; Yang, R. Preparation and electrocatalytic activity of 3D hierarchical porous spinel CoFe₂O₄ hollow nanospheres as efficient catalyst for oxygen reduction reaction and oxygen evolution reaction. *Electrochim. Acta* **2015**, *151*, 276–283. [[CrossRef](#)]
102. Yan, W.; Cao, X.; Ke, K.; Tian, J.; Jin, C.; Yang, R. One-pot synthesis of monodispersed porous CoFe₂O₄ nanospheres on graphene as an efficient electrocatalyst for oxygen reduction and evolution reactions. *RSC Adv.* **2016**, *6*, 307–313. [[CrossRef](#)]
103. Yan, W.; Yang, Z.; Bian, W.; Yang, R. FeCo₂O₄/hollow graphene spheres hybrid with enhanced electrocatalytic activities for oxygen reduction and oxygen evolution reaction. *Carbon* **2015**, *92*, 74–83. [[CrossRef](#)]
104. Zhao, X.; Fu, Y.; Wang, J.; Xu, Y.; Tian, J.-H.; Yang, R. Ni-doped CoFe₂O₄ Hollow Nanospheres as Efficient Bi-functional Catalysts. *Electrochim. Acta* **2016**, *201*, 172–178. [[CrossRef](#)]
105. Liu, S.; Bian, W.; Yang, Z.; Tian, J.; Jin, C.; Shen, M.; Zhou, Z.; Yang, R. A facile synthesis of CoFe₂O₄/biocarbon nanocomposites as efficient bi-functional electrocatalysts for the oxygen reduction and oxygen evolution reaction. *J. Mater. Chem. A* **2014**, *2*, 18012–18017. [[CrossRef](#)]
106. Li, P.; Ma, R.; Zhou, Y.; Chen, Y.; Zhou, Z.; Liu, G.; Liu, Q.; Peng, G.; Liang, Z.; Wang, J. In situ growth of spinel CoFe₂O₄ nanoparticles on rod-like ordered mesoporous carbon for bifunctional electrocatalysis of both oxygen reduction and oxygen evolution. *J. Mater. Chem. A* **2015**, *3*, 15598–15606. [[CrossRef](#)]
107. Yan, W.; Bian, W.; Jin, C.; Tian, J.-H.; Yang, R. An Efficient Bi-functional Electrocatalyst Based on Strongly Coupled CoFe₂O₄/Carbon Nanotubes Hybrid for Oxygen Reduction and Oxygen Evolution. *Electrochim. Acta* **2015**, *177*, 65–72. [[CrossRef](#)]
108. Bian, W.; Yang, Z.; Strasser, P.; Yang, R. A CoFe₂O₄/graphene nano hybrid as an efficient bi-functional electrocatalyst for oxygen reduction and oxygen evolution. *J. Power Sources* **2014**, *250*, 196–203. [[CrossRef](#)]
109. Yan, W.; Cao, X.; Tian, J.; Jin, C.; Ke, K.; Yang, R. Nitrogen/sulfur dual-doped 3D reduced graphene oxide networks-supported CoFe₂O₄ with enhanced electrocatalytic activities for oxygen reduction and evolution reactions. *Carbon* **2016**, *99*, 195–202. [[CrossRef](#)]
110. Wang, Y.; Liu, Q.; Zhang, L.; Hu, T.; Liu, W.; Liu, N.; Du, F.; Li, Q.; Wang, Y. One-pot synthesis of Ag-CoFe₂O₄/C as efficient catalyst for oxygen reduction in alkaline media. *Int. J. Hydrog. Energy* **2016**, *41*, 22547–22553. [[CrossRef](#)]
111. Huo, R.; Jiang, W.-J.; Xu, S.; Zhang, F.; Hu, J.-S. Co/CoO/CoFe₂O₄/G nanocomposites derived from layered double hydroxides towards mass production of efficient Pt-free electrocatalysts for oxygen reduction reaction. *Nanoscale* **2014**, *6*, 203–206. [[CrossRef](#)] [[PubMed](#)]
112. Wang, Y.; Liu, Q.; Hu, T.; Zhang, L.; Deng, Y. Carbon supported MnO₂-CoFe₂O₄ with enhanced electrocatalytic activity for oxygen reduction and oxygen evolution. *Appl. Surf. Sci.* **2017**, *403*, 51–56. [[CrossRef](#)]

